Synchrotrotron Radiation in the LHC Experimental Insertions

F. Zimmermann

June 19, 2003

1 Introduction

In order to assist in the finalization of the design for the vacuum chamber in the LHC insertion regions, we have performed a series of simulations with the code PHOTON [1], by which we estimated the photon flux and energies of incident photons all along the 4 long straight sections around IP1, IP2, IP5 and IP8. In particular, we investigated the effect of a sawtooth chamber in this region.

We assume the classical formula of synchrotron radiation, ignoring magnet edge effects [2] and any shielding by the vacuum chamber.

2 Apertures

In the present LHC MAD database, certain magnet apertures are already included. Aperture values are available for the bending magnets and quadrupoles outside the arcs (including the proper orientation of the beam screen where present). Unfortunately these amount to only a small fraction of the total number of 11616 elements, which are listed in the optics file. Especially, apertures are defined neither for the drifts nor for collimators.

For the arcs, we have assumed half apertures of 22.02 mm and 17.14 mm (beam screen) [3]. In addition, over $\pm$260 m around each IP, we have used the following approximate description for all undefined apertures (notably the drifts):

- IP 1: 0–19.05 m from the IP circular aperture of radius 30 mm, 19.05–86 m from the IP circular aperture of radius 40 mm, 86–140 m from the IP circular aperture of radius 106 mm, 140–260 m from the IP circular aperture of radius 40 mm
- IP 5: 0–19.05 m from the IP circular aperture of radius 30 mm, 19.05–86 m from the IP circular aperture of radius 40 mm, 86–140 m from the IP circular aperture of radius 106 mm, 140–260 m from the IP circular aperture of radius 40 mm
- IP 2: 0–19 m from the IP circular aperture of radius 30 mm, 19.05–73 m from the IP circular aperture of radius 40 mm, 73–112 m from the IP circular aperture of radius 106 mm, 112–260 m from the IP circular aperture of radius 40 mm
- IP 8: 0–0.5 m from the IP circular aperture of radius 6 mm, 0.5–19 m from the IP circular aperture of radius 30 mm, 19.05–73 m from the IP circular aperture of radius 40 mm, 73–112 m from the IP circular aperture of radius 106 mm, 112–260 m from the IP circular aperture of radius 40 mm.

The apertures around the four IPs so obtained are displayed in Fig. 1. The IPs are always at zero. For completeness and later reference, the original coordinates of the IP positions in the MAD file are 0 and/or 266658.88 m for IP1, 3332.437 m for IP2, 13329.289 m for IP5, and 23315.38 m for IP8.

3 Simulation Parameters and Results

Simulations were performend for LHC optics version 6.4, including the nominal crossing angles at all 4 IPs. We treated one beam at a time, usually beam 1, which moves clockwise around the ring. Beam parameters are specified in Table 1. For each of 5 different random seeds (characterizing the synchrotron radiation: the 3-dim. emission point, the photon energy and the initial momentum direction) we tracked 10^{10} photons. An error estimate is obtained from the variation across the seeds. Synchrotron radiation from quadrupole magnets is included, as described in [1]. We assumed an initial intrinsic photon angular distribution of Gaussian shape with a width of $1/\gamma$.

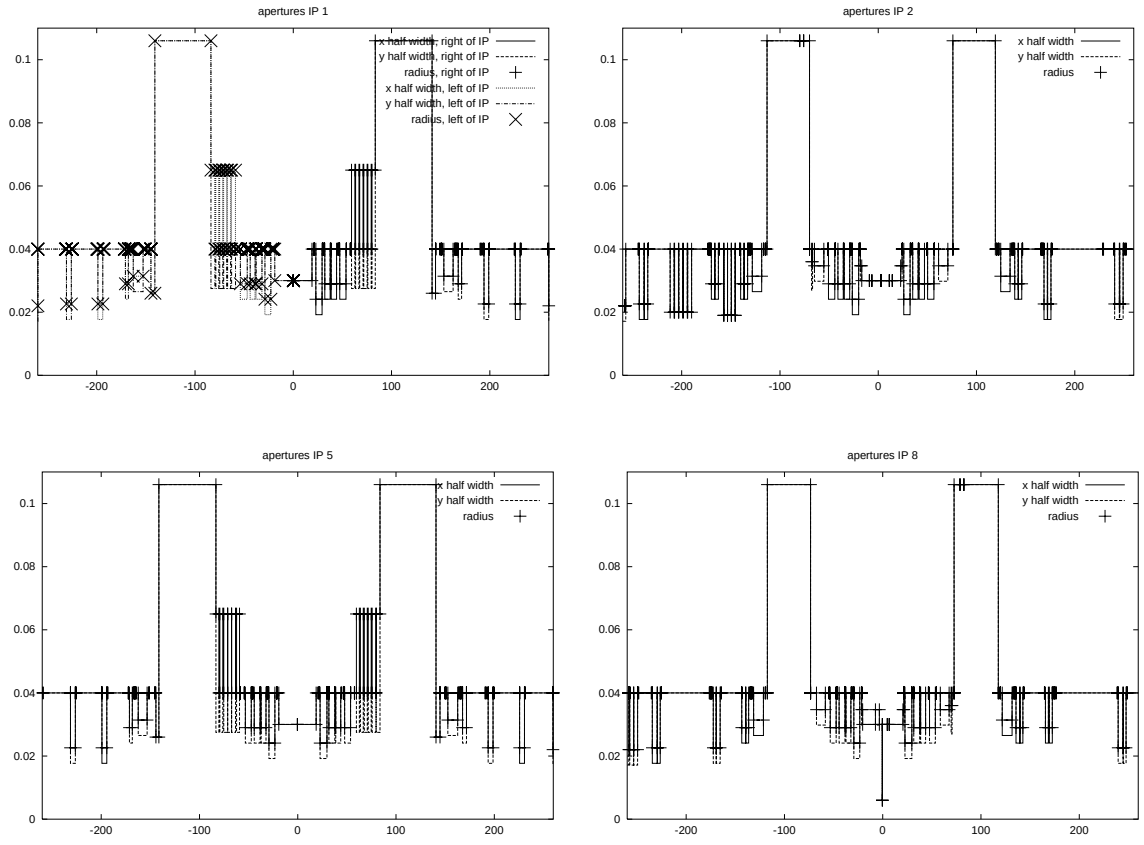

Figure 1: Apertures around the four IPs.

Table 1: Beam parameters.

parameter	symbol	value
energy	E	7 TeV
rel. factor	γ	7461
norm. emittance	$\gamma\epsilon_{x,y}$	3.75 μm
rms momentum spread	$\delta_{\rm rms}$	1.11×10^{-4}
number of bunches	n_b	2808
particles per bunch	N_b	1.1×10^{11}
circumference	C	26659 m

3.1 Effect of Reflectivity

To unveil the effect that a sawtooth chamber in the long-straight sections might have, we compare results obtained for two different reflectivities over the full length of the straight section (two times 260 m), namely 0.8 and 0.02.

First, we considered the ideal machine without additional errors. Figures 2 and 3 show the photon flux per second for the various beam line elements around each IP and the different reflectivities. We decided to plot the flux as a function of element rather than normalized per unit length, since the lengths of different elements (of different apertures) may differ widely in the straight sections.

The effect of reducing the reflectivity is not strong. Sometimes it increases and sometimes it lowers the flux, depending on the position among the beam line. This is further illustrated in Fig. 4 which superimposes the results for $R = 0.80$ and $R = 0.02$ around IP5 and IP8.

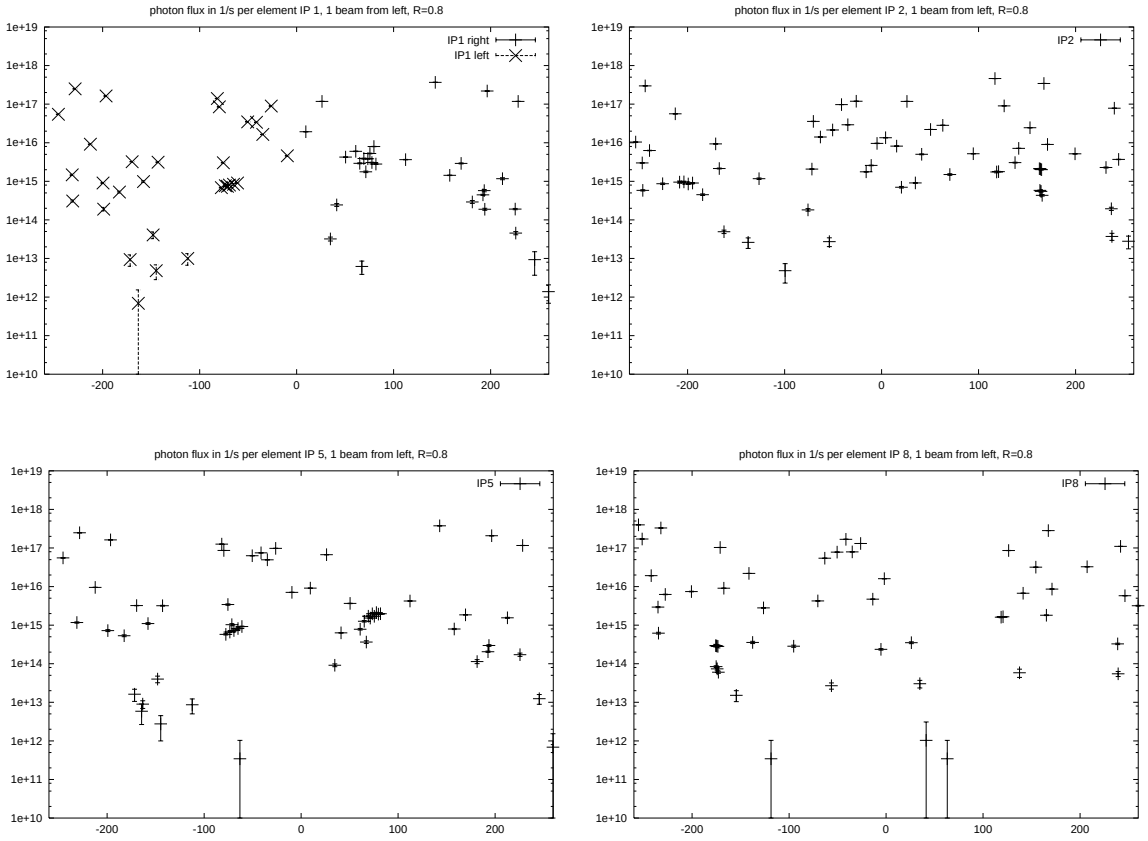

Figure 2: Photon flux per element for a reflectivity $R = 0.8$.

Figures 5 and 6 depict the average photon energies, again for the two different reflectivities.
Figures 7 and 8 display the average heat loads per element, in units of W, again for the 4 IPs.

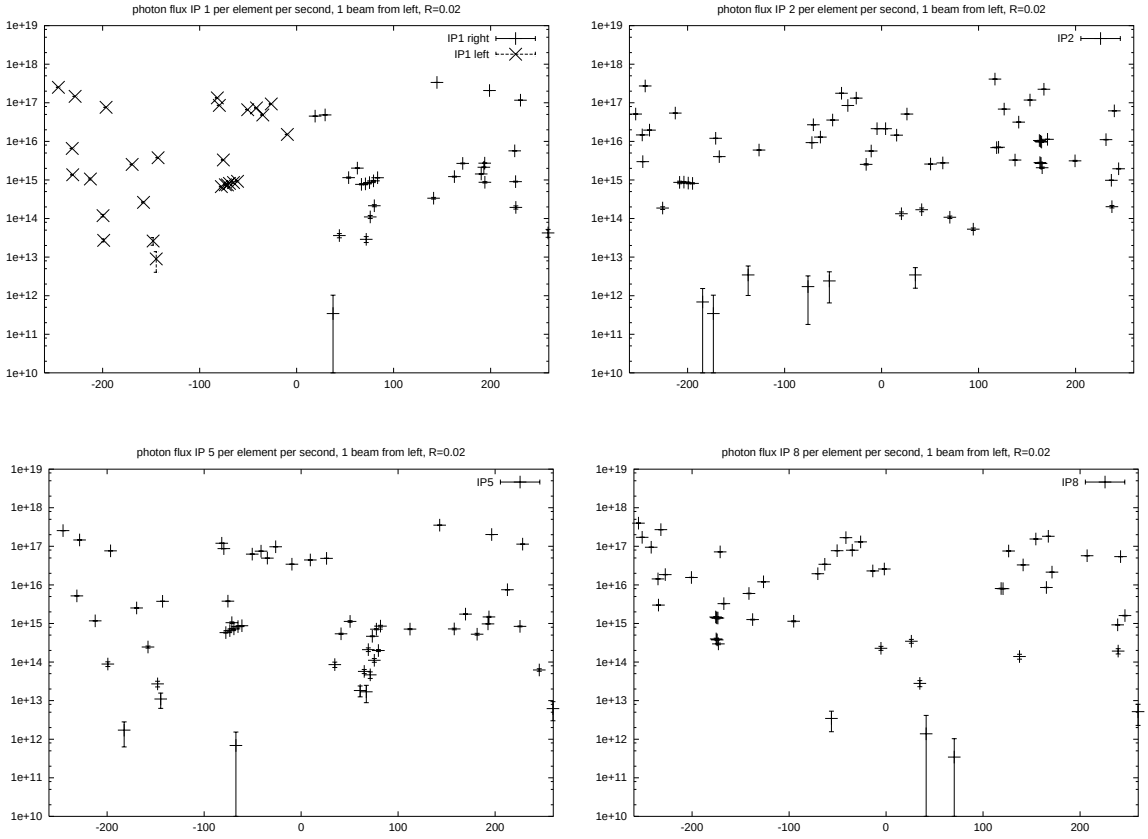

Figure 3: Photon flux per element for a reflecivity $R = 0.02$.

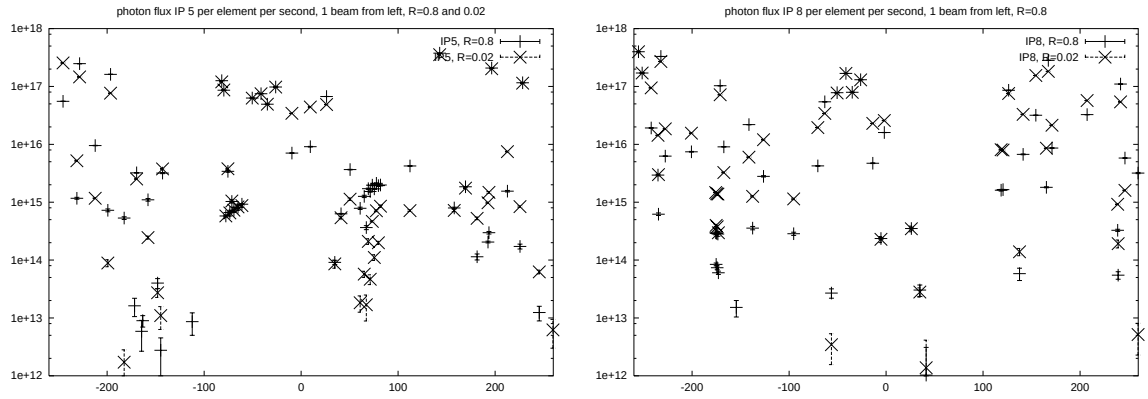

Figure 4: Photon flux per element at IP5 (left) and IP8 (right), directly comparing the two reflecivities of $R = 0.02$ and $R = 0.80$.

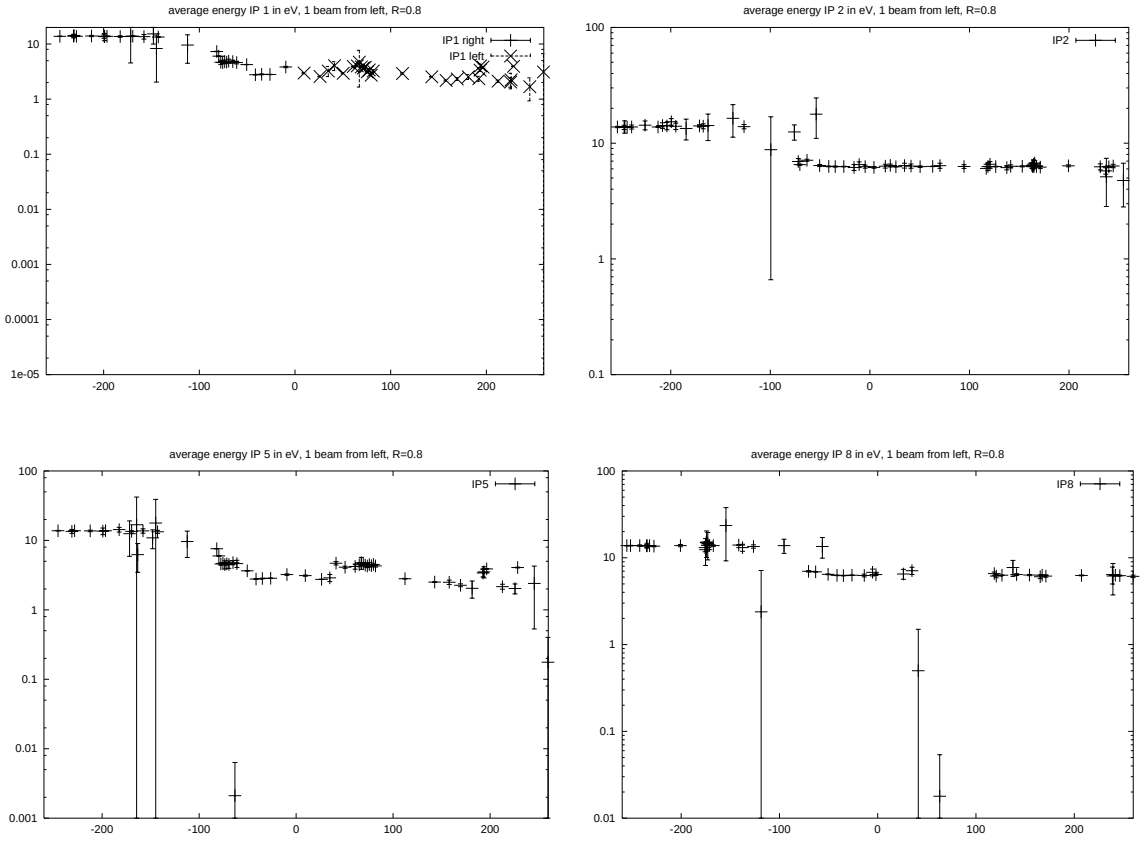

Figure 5: Average photon energy per element in eV for a reflectivity $R = 0.8$.

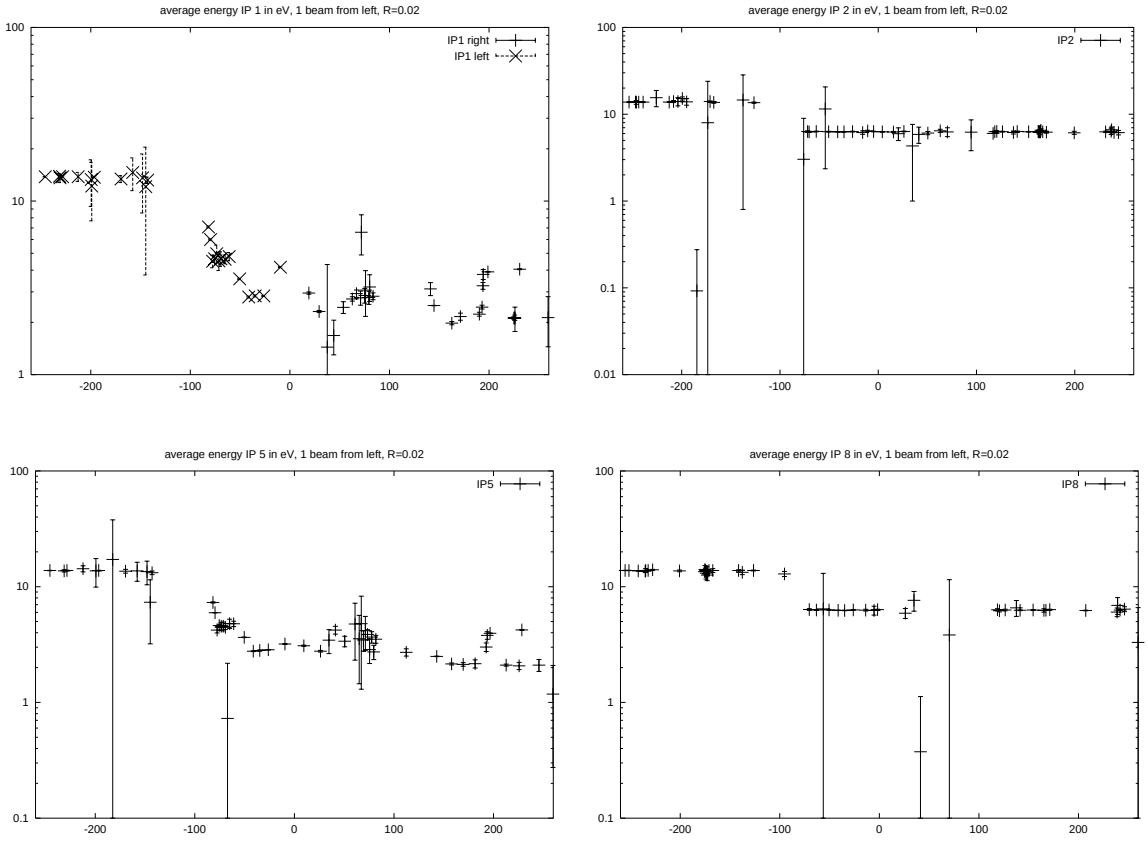

Figure 6: Average photon energy element in eV for a reflecivity $R = 0.02$.

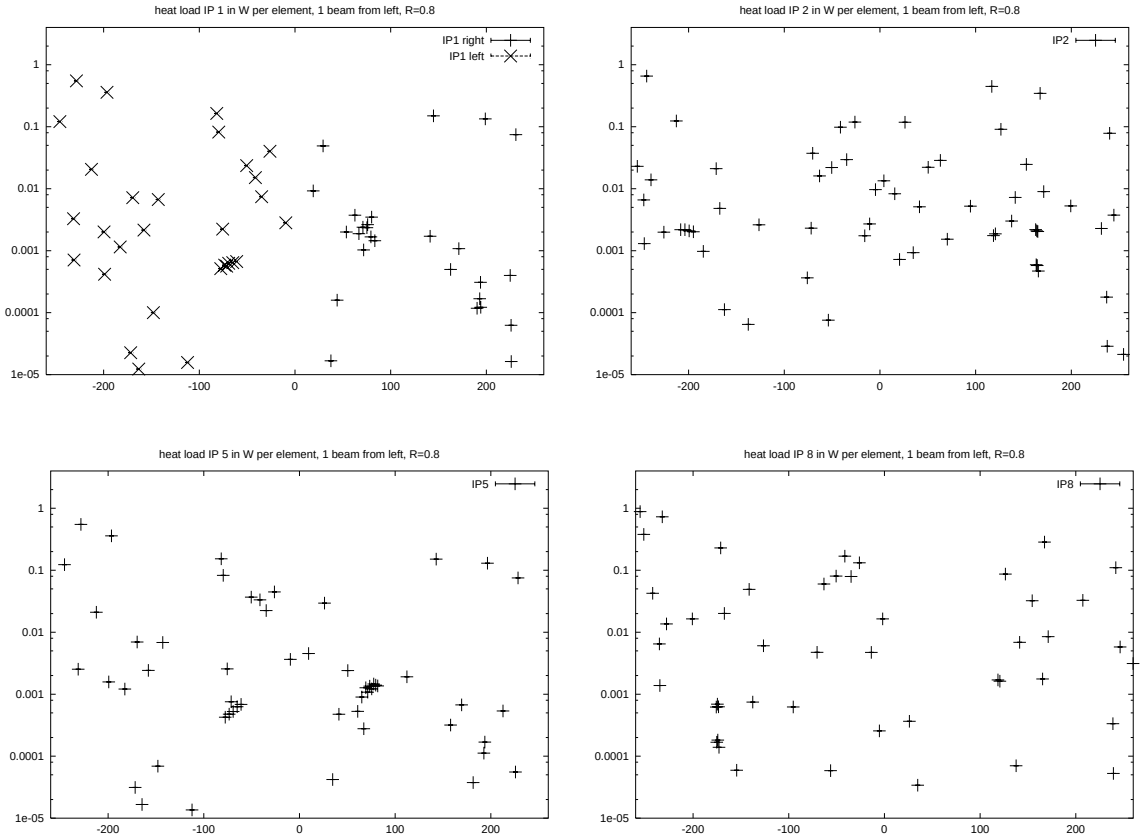

Figure 7: Heat load per element for a reflectivity $R = 0.8$.

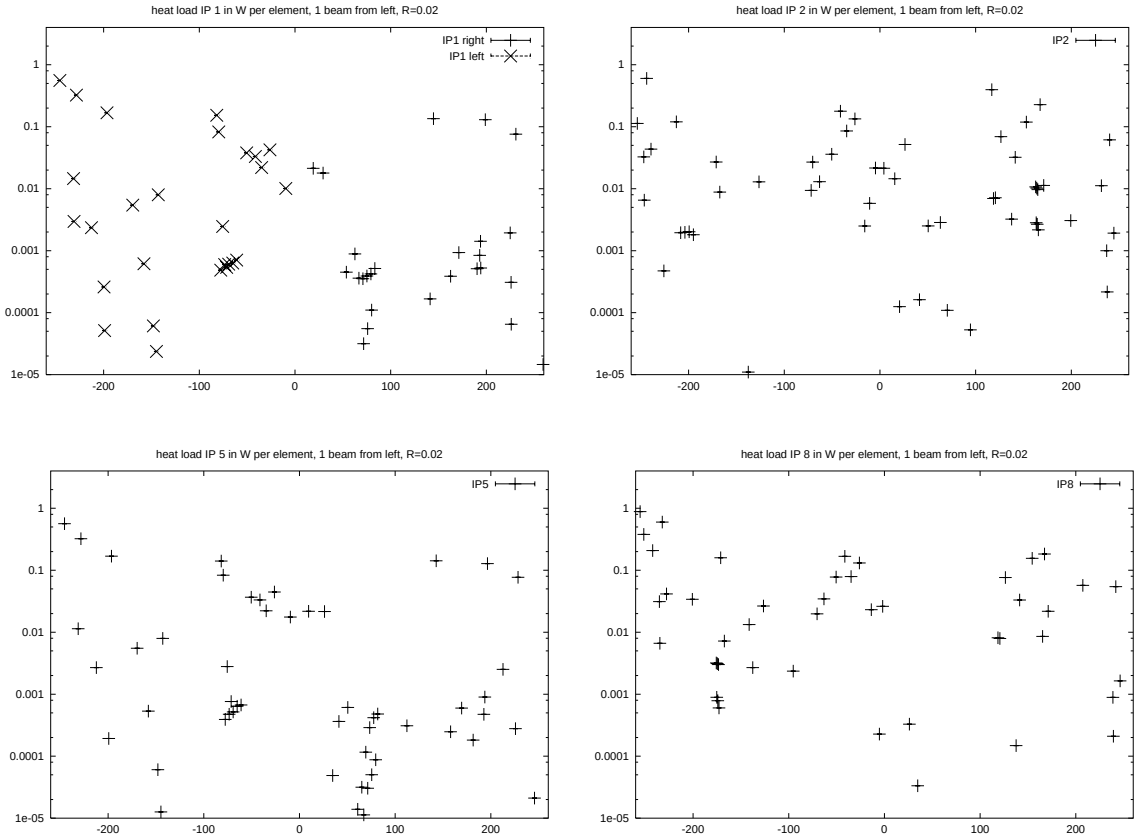

Figure 8: Heat load per element for a reflectivity $R = 0.02$.

3.2 Second Beam

We have performed the same simulation for beam 2, which moves from the right to the left. (To do so, in MADX we used the flag $BV = -1$ for the definition of beam 2, and we reflected the sequence, in seqedit, after flattening it.) The resulting photon flux per element are displayed in Fig. 9, which should be compared with the analogous results for beam 1 in Fig. 2. There is no obvious (mirror) symmetry between the two, and in most cases it appears as if for beam 2 less points are hit by the syenchotron light on the outgoing side.

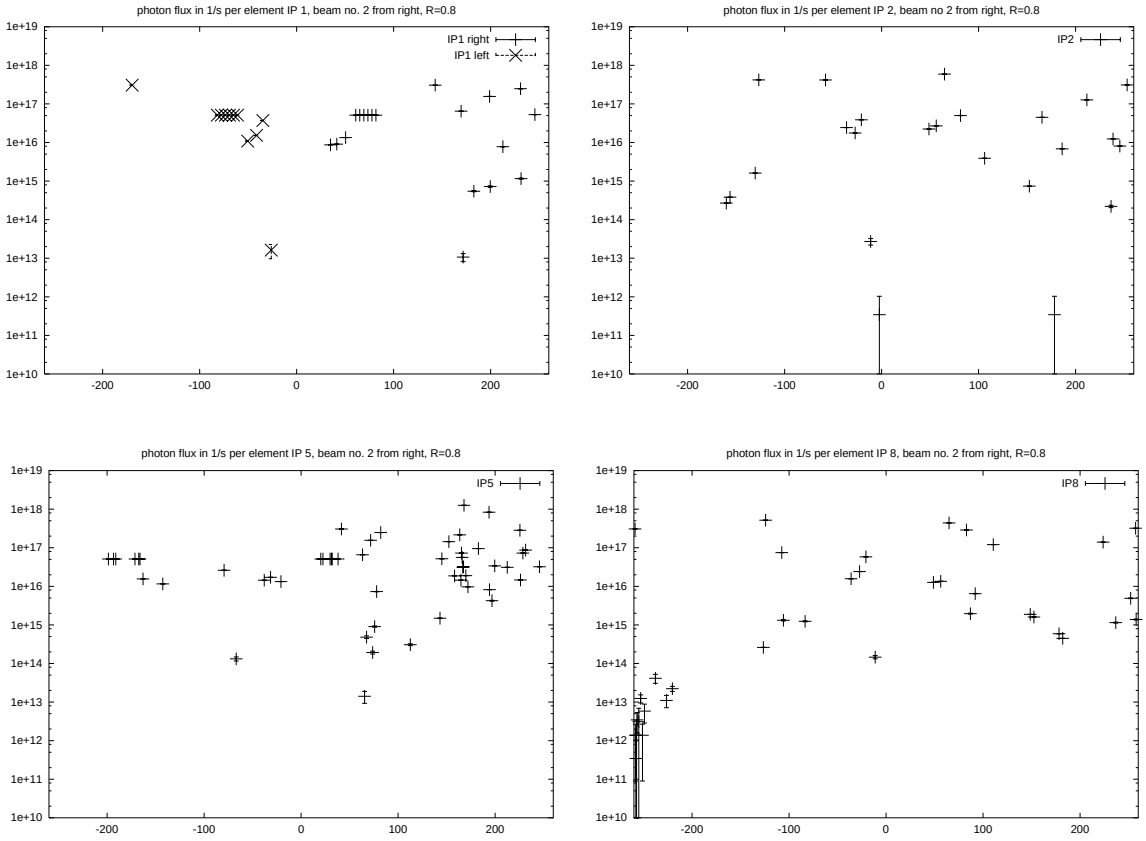

Figure 9: Photon flux per element due to beam 2, coming from the right, for a reflectivity $R = 0.8$.

3.3 Radiation from Quadrupoles

Figure 10 compares photon flux and heat load from all dipoles and quadrupoles with that from the dipoles alone. The figure illustrates that the synchrotron radiation from quadrupoles is a marginal effect.

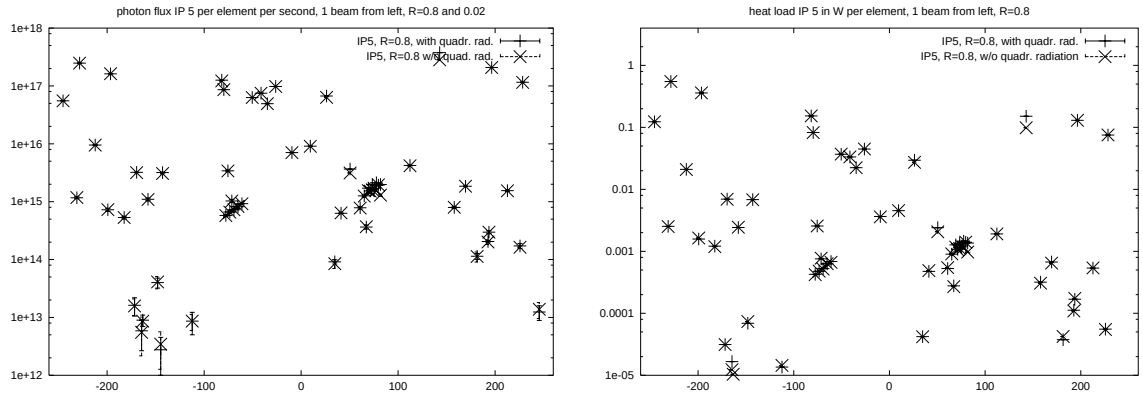

Figure 10: Photon flux in 1/s (left), and heat load in W (right) per element near IP5 for a photon reflectivity $R = 0.8$, comparing radiation in quadrupoles and dipoles with that in dipoles only.

3.4 Radiation Angle at Low Energy

At low energies the angular distribution of the photons in the vertical plane is no longer like $1/\gamma$ but rather like $(E_c/E_\gamma)^{1/3}/\gamma$. Assuming this distribution throughout (*i.e*, for all photon energies), we can study the effect of such details on the photon flux and heat load. The differences to the $1/\gamma$ case are shown in Fig. 11 for both the flux and heat load per element. At most places, especially for regions with high flux rates, the difference is small, but in some location, close to and behind the IP, we do observe a significant dependence on the initial photon angular distribution.

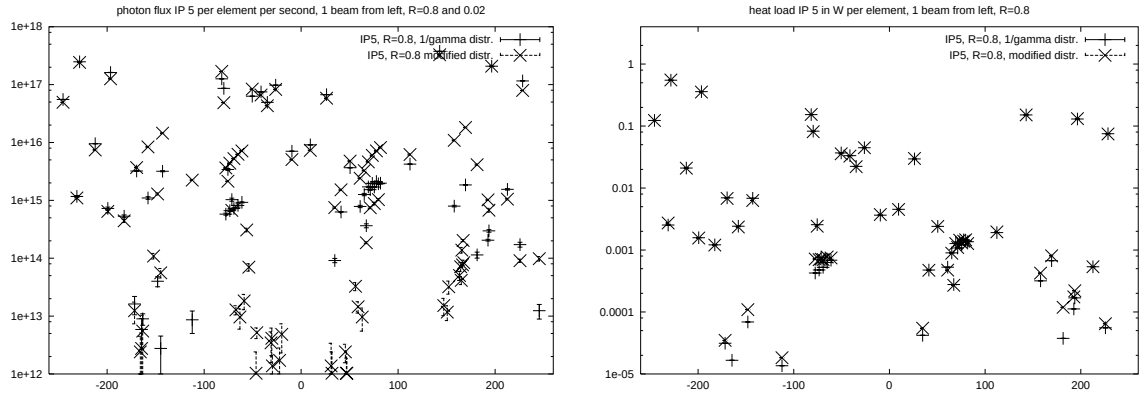

Figure 11: Photon flux in 1/s (left), and heat load in W (right) per element near IP5 for a photon reflectivity $R = 0.8$, comparing two different vertical angular distributions for the photon emission.

3.5 Optics Errors

To investigate the effect of optics errors of the photon distribution, we have randomly misaligned all quadrupoles of type MQ by 500 μm rms in the horizontal and vertical direction, and, also for these quadrupoles, we have introduced random field errors of 2% rms. Subsequently, we have corrected the orbit to an rms value of about 1 mm in both planes, using an SVD-conditioned micado algorithm [5]. Prior to the orbit correction, we deactivated all kickers, crossing-angle correctors and spectrometer elements of type MBLW, MBXWH, MBXWS, MBXWT, MSDB, MKA, MCBYH, MCBYV, MCBX, MBAW.R2, MBWMD.1L2, MKI, MKD, MKQ, MSDA, MSDB, MSDB2, MSDC, MSIA, and MSIB, least these not be employed for correcting the orbit.

Figure 12 illustrates the impact of the optics errors on the beam orbit, the beta function and the horizontal dispersion around each of teh four IPs.

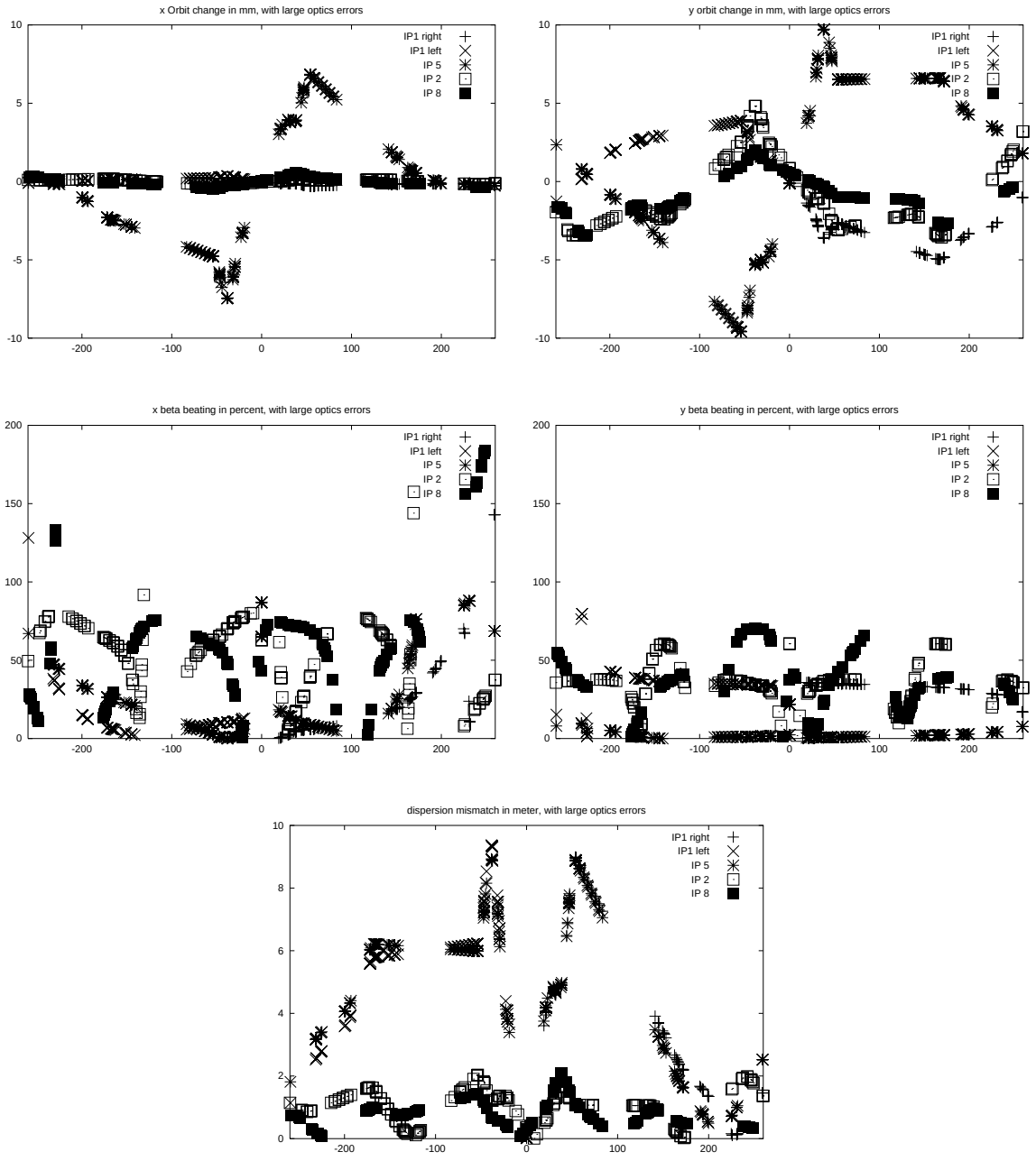

Figure 12: Horizontal and vertical orbit change (top), beta beating (center), and horizontal dispersion mismatch (bottom) near each of the four IPs due to large optics errors we introduced in the simulation.

Figure 13 shows the photon flux simulated in the presence of optics errors. It should be compared with the

results of the analogous simulation for the ideal optics. in Fig. 2.

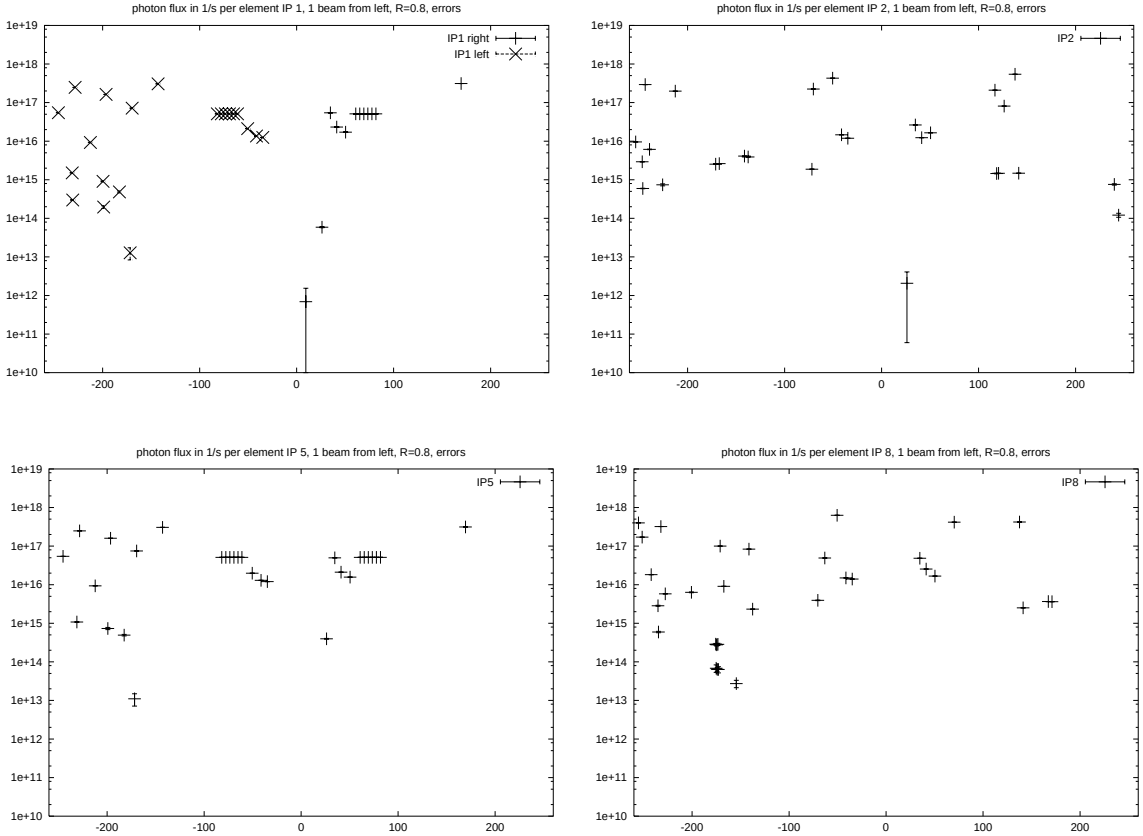

Figure 13: Photon flux per element for a reflectivity $R = 0.8$ and including optics errors.

3.6 Summary of Results

Table 2: Simulated photon flux per meter and second around each IP from a single beam. Error indicates rms variation with synchrotron-radiation random seed.

case	IP	-260 to -100 m	-100 to 0m	0 to 100 m	100 to 260 m
beam 1,	IP1	$3.0 \times 10^{15} \pm 6 \times 10^{12}$	$4.1 \times 10^{15} \pm 6 \times 10^{12}$	$1.8 \times 10^{15} \pm 6 \times 10^{12}$	$4.5 \times 10^{15} \pm 4 \times 10^{12}$
$R = 0.8$	IP2	$2.5 \times 10^{15} \pm 5 \times 10^{12}$	$3.3 \times 10^{15} \pm 7 \times 10^{12}$	$2.0 \times 10^{15} \pm 3 \times 10^{12}$	$6.5 \times 10^{15} \pm 6 \times 10^{12}$
	IP5	$3.0 \times 10^{15} \pm 6 \times 10^{12}$	$5.1 \times 10^{15} \pm 8 \times 10^{12}$	$9.6 \times 10^{14} \pm 3 \times 10^{12}$	$4.4 \times 10^{15} \pm 4 \times 10^{12}$
	IP8	$6.7 \times 10^{15} \pm 9 \times 10^{12}$	$5.4 \times 10^{15} \pm 7 \times 10^{12}$	$3.8 \times 10^{12} \pm 2 \times 10^{11}$	$3.6 \times 10^{15} \pm 5 \times 10^{12}$
beam 1,	IP1	$3.1 \times 10^{15} \pm 6 \times 10^{12}$	$5.2 \times 10^{15} \pm 8 \times 10^{12}$	$1.0 \times 10^{15} \pm 2 \times 10^{12}$	$4.2 \times 10^{15} \pm 4 \times 10^{12}$
$R = 0.02$	IP2	$2.8 \times 10^{15} \pm 4 \times 10^{12}$	$5.1 \times 10^{15} \pm 6 \times 10^{12}$	$9.3 \times 10^{14} \pm 3 \times 10^{12}$	$6.3 \times 10^{15} \pm 6 \times 10^{12}$
	IP5	$3.1 \times 10^{15} \pm 5 \times 10^{12}$	$5.4 \times 10^{15} \pm 9 \times 10^{12}$	$9.7 \times 10^{14} \pm 4 \times 10^{12}$	$4.3 \times 10^{15} \pm 4 \times 10^{12}$
	IP8	$6.8 \times 10^{15} \pm 9 \times 10^{12}$	$5.6 \times 10^{15} \pm 7 \times 10^{12}$	$3.8 \times 10^{12} \pm 4 \times 1011$	$3.8 \times 10^{15} \pm 3 \times 10^{12}$
beam 1,	IP1	$2.9 \times 10^{15} \pm 4 \times 10^{12}$	$4.2 \times 10^{15} \pm 7 \times 10^{12}$	$1.8 \times 10^{15} \pm 5 \times 10^{12}$	$4.3 \times 10^{15} \pm 5 \times 10^{12}$
$R = 0.8$,	IP2	$2.2 \times 10^{15} \pm 4 \times 10^{12}$	$3.6 \times 10^{15} \pm 6 \times 10^{12}$	$2.1 \times 10^{15} \pm 6 \times 10^{12}$	$6.2 \times 10^{15} \pm 5 \times 10^{12}$
mod.	IP5	$2.9 \times 10^{15} \pm 5 \times 10^{12}$	$5.3 \times 10^{15} \pm 8 \times 10^{12}$	$1.1 \times 10^{15} \pm 3 \times 10^{12}$	$4.1 \times 10^{15} \pm 4 \times 10^{12}$
angle	IP8	$6.4 \times 10^{15} \pm 5 \times 10^{12}$	$5.5 \times 10^{15} \pm 9 \times 10^{12}$	$2.4 \times 10^{14} \pm 2 \times 10^{12}$	$3.5 \times 10^{15} \pm 6 \times 10^{12}$
beam 1,	IP1	$3.0 \times 10^{15} \pm 6 \times 10^{12}$	$4.1 \times 10^{15} \pm 7 \times 10^{12}$	$1.7 \times 10^{15} \pm 5 \times 10^{12}$	$3.9 \times 10^{15} \pm 4 \times 10^{12}$
$R = 0.8$,	IP2	$2.4 \times 10^{15} \pm 5 \times 10^{12}$	$3.3 \times 10^{15} \pm 7 \times 10^{12}$	$2.0 \times 10^{15} \pm 2 \times 10^{12}$	$5.6 \times 10^{15} \pm 7 \times 10^{12}$
only	IP5	$3.0 \times 10^{15} \pm 5 \times 10^{12}$	$5.1 \times 10^{15} \pm 7 \times 10^{12}$	$9.0 \times 10^{14} \pm 3 \times 10^{12}$	$3.8 \times 10^{15} \pm 5 \times 10^{12}$
dipoles	IP8	$6.7 \times 10^{15} \pm 7 \times 10^{12}$	$5.3 \times 10^{15} \pm 9 \times 10^{12}$	$3.9 \times 10^{12} \pm 2 \times 10^{11}$	$3.6 \times 10^{15} \pm 7 \times 10^{12}$
beam 1,	IP1	$5.3 \times 10^{15} \pm 6 \times 10^{12}$	$3.5 \times 10^{15} \pm 5 \times 10^{6}$	$4.0 \times 10^{15} \pm 2 \times 10^{10}$	$2.0 \times 10^{15} \pm 4 \times 10^{6}$
$R = 0.8$,	IP2	$3.3 \times 10^{15} \pm 4 \times 10^{12}$	$6.8 \times 10^{15} \pm 9 \times 10^{12}$	$5.5 \times 10^{14} \pm 2 \times 10^{10}$	$5.3 \times 10^{15} \pm 6 \times 10^{12}$
errors	IP5	$5.3 \times 10^{15} \pm 4 \times 10^{12}$	$3.5 \times 10^{15} \pm 5 \times 10^{6}$	$3.9 \times 10^{15} \pm 4 \times 10^{11}$	$2.7 \times 10^{15} \pm 2 \times 10^{6}$
	IP8	$7.0 \times 10^{15} \pm 1 \times 10^{13}$	$7.1 \times 10^{15} \pm 5 \times 10^{12}$	$5.1 \times 10^{15} \pm 2 \times 10^{7}$	$2.7 \times 10^{15} \pm 1 \times 10^{7}$
beam 2,	IP1	$1.9 \times 10^{15} \pm 6 \times 10^{12}$	$3.7 \times 10^{15} \pm 4 \times 10^{6}$	$3.4 \times 10^{15} \pm 7 \times 10^{10}$	$5.2 \times 10^{15} \pm 1 \times 10^{7}$
$R = 0.8$	IP2	$2.6 \times 10^{15} \pm 6 \times 10^{12}$	$5.0 \times 10^{15} \pm 4 \times 10^{12}$	$6.9 \times 10^{15} \pm 6 \times 10^{11}$	$3.2 \times 10^{15} \pm 4 \times 10^{12}$
	IP5	$2.1 \times 10^{15} \pm 1 \times 10^{13}$	$7.1 \times 10^{14} \pm 7 \times 10^{12}$	$1.1 \times 10^{16} \pm 4 \times 10^{11}$	$2.1 \times 10^{16} \pm 3 \times 10^{6}$
	IP8	$5.6 \times 10^{15} \pm 8 \times 10^{12}$	$9.9 \times 10^{14} \pm 6 \times 10^{12}$	$7.6 \times 10^{15} \pm 4 \times 10^{11}$	$3.7 \times 10^{15} \pm 3 \times 10^{7}$

3.7 LHC Arcs

For completeness, Fig. 14 shows the photon flux and heat load all around the LHC. The results for the arcs agree with those in Ref. [1].

4 Conclusion

5 Acknowledgement

We thank W. Herr, B. Jeanneret, and F. Schmidt for useful discussions.

Table 3: Simulated average energy of impacting photons around each IP in eV for a single beam. Statistical errors are negligibly small.

case	IP	−260 to −100 m	−100 to 0m	0 to 100 m	100 to 260 m
beam 1,	IP1	13.8	5.2	2.8	3.2
$R = 0.8$	IP2	13.8	6.4	6.3	6.2
	IP5	13.8	4.7	3.1	3.2
	IP8	13.8	6.4	6.5	6.3
beam 1,	IP1	13.8	4.6	2.6	3.2
$R = 0.02$	IP2	13.8	6.3	6.3	6.2
	IP5	13.8	4.5	2.9	3.2
	IP8	13.8	6.3	6.0	6.3
beam 1,	IP1	14.7	5.0	2.8	3.3
$R = 0.8$,	IP2	15.1	6.0	6.0	6.5
mod. angle	IP5	14.6	4.5	2.8	3.4
	IP8	14.5	6.2	0.2	6.5
beam 1,	IP1	13.8	5.2	2.79	3.1
$R = 0.8$,	IP2	13.8	6.4	6.3	6.3
only dipoles	IP5	13.8	4.7	3.1	3.1
	IP8	13.8	6.4	6.3	6.3
beam 1,	IP1	10.3	2.5	2.9	4.5
$R = 0.8$,	IP2	13.1	6.1	3.3	6.3
errors	IP5	10.3	2.5	2.8	4.5
	IP8	13.6	6.2	6.3	6.1
beam 2,	IP1	4.6	2.4	2.2	10.4
$R = 0.8$	IP2	6.2	6.0	6.3	13.7
	IP5	2.2	3.6	7.9	13.8
	IP8	8.8	5.9	6.2	12.1

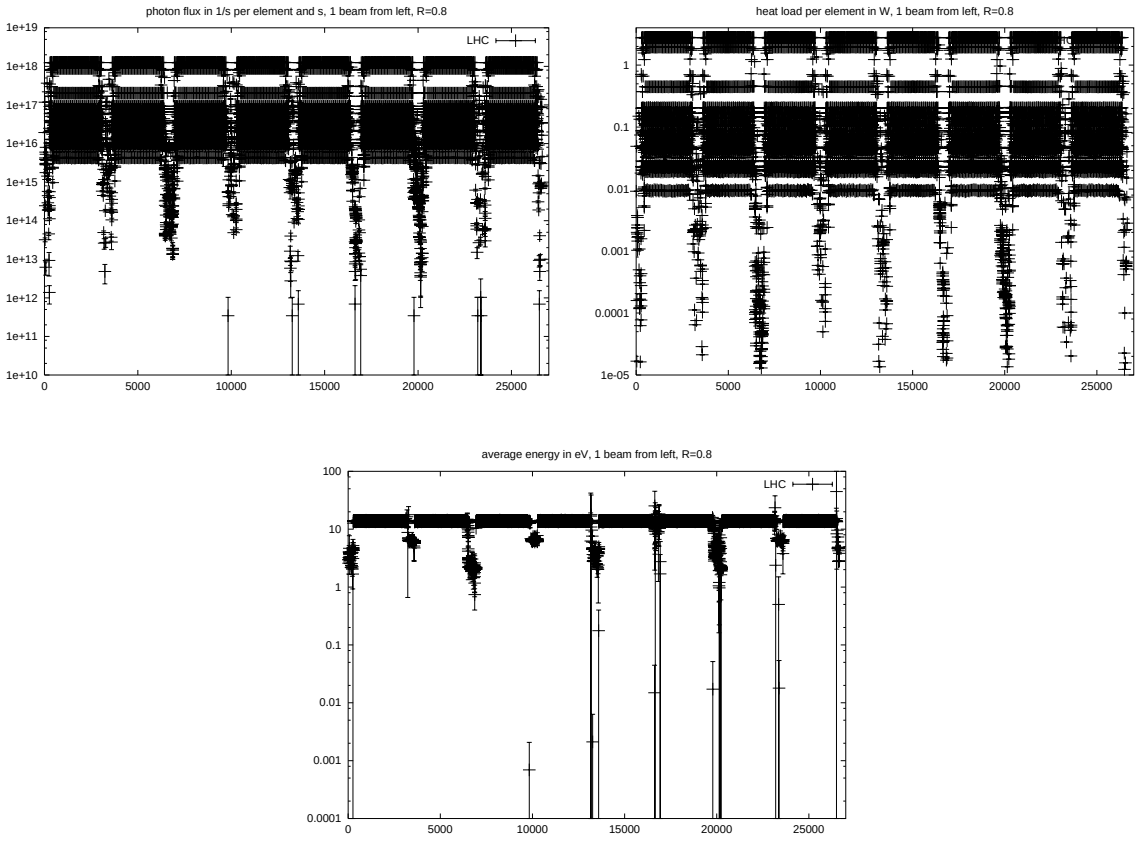

Figure 14: Photon flux in 1/s, heat load in W, and average photon energy in eV, per element all around the LHC for a photon reflectivity $R = 0.8$ in the LSS and $R = 0.02$ in the arcs.

A Corrections to LHC Project Note 237

The formulae (16)–(21) in Ref. [1] contain some errors and typos. They must be corrected as follows.

The reflection transformations read:

$$x_{\rm new} = x_{\rm old} - 2n_x d\vec{p}\cdot\vec{n} \quad (1)$$

$$y_{\rm new} = y_{\rm old} - 2n_y d\vec{p}\cdot\vec{n} \quad (2)$$

$$x'_{\rm new} = x'_{\rm old} - 2n_x \vec{p}\cdot\vec{n} \quad (3)$$

$$y'_{\rm new} = y'_{\rm old} - 2n_y \vec{p}\cdot\vec{n} \quad (4)$$

where $\vec{p} = (x'_{rmold}, y'_{\rm old})$ is the transverse slope of the initial photon momentum,

$$\vec{n} = \begin{pmatrix} n_x \\ n_y \end{pmatrix} = \begin{pmatrix} x_i b^2/\sqrt{x_i^2 b^4 + y_i^2 x^4} \\ y_i a^2/\sqrt{x_i^2 b^4 + y_i^2 x^4} \end{pmatrix} , \quad (5)$$

the transverse normal vector at the point of impact $(x_i, y_i) = (x_{\rm old} - dx'_{\rm old}, y_{\rm old} - dy'_{\rm old})$, and the parameter

$$d = \left|\frac{B}{A}\right| - \frac{1}{A}\sqrt{B^2 - CA} \quad (6)$$

with

$$A = \frac{x'^2_{\rm old}}{a^2} + \frac{y'^2_{\rm old}}{b^2} \quad (7)$$

$$B = \frac{x'_{\rm old} x_{\rm old}}{a^2} + \frac{y'_{\rm old} y_{\rm old}}{b^2} \quad (8)$$

$$C = \frac{x^2_{\rm old}}{a^2} + \frac{y^2_{\rm old}}{b^2} - 1 , \quad (9)$$

where a and b refer to the horizontal and vertical semi-axes of an elliptical beam pipe.

References

[1] F. Zimmermann, "Synchrotron Radiation in the LHC Arcs — Monte-Carlo Approach," LHC Project Note 237 (2000).

[2] H. Burkhardt, "Reminder of the Edge Effect in Synchrotron Radiation," LHC Project Note 172 (1998).

[3] B. Jeanneret, private communication (2003).

[4] G. Stupakov. "Theory and Observation of Microbunching Instability in Electron Machines," PAC 2003, Portland (2003).

[5] W. Herr, "Implementation of New Closed Orbit Correction Procedures in the MAD-X program," CERN-SL-2002-48 (AP).